In vivo analysis of outer arm dynein transport reveals cargo-specific intraflagellar transport properties

Jin Dai[a], Francesco Barbieri[a,b], David R. Mitchell[c,*], and Karl F. Lechtreck[a,*]
[a]Department of Cellular Biology, University of Georgia, Athens, GA 30602; [b]Department of Life Science, University of Siena, 53100 Siena, Italy; [c]Department of Cell and Developmental Biology, SUNY Upstate Medical University, Syracuse, NY 13210

ABSTRACT **Outer dynein arms (ODAs) are multiprotein complexes that drive flagellar beating. Based on genetic and biochemical analyses, ODAs preassemble in the cell body and then move into the flagellum by intraflagellar transport (IFT). To study ODA transport in vivo, we expressed the essential intermediate chain 2 tagged with mNeonGreen (IC2-NG) to rescue the corresponding *Chlamydomonas reinhardtii* mutant *oda6*. IC2-NG moved by IFT; the transport was of low processivity and increased in frequency during flagellar growth. As expected, IFT of IC2-NG was diminished in *oda16*, lacking an ODA-specific IFT adapter, and in *ift46 IFT46ΔN* lacking the ODA16-interacting portion of IFT46. IFT loading appears to involve ODA16-dependent recruitment of ODAs to basal bodies followed by handover to IFT. Upon unloading from IFT, ODAs rapidly docked to the axoneme. Transient docking still occurred in the docking complex mutant *oda3* indicating that the docking complex stabilizes rather than initiates ODA–microtubule interactions. In full-length flagella, ODAs continued to enter and move inside cilia by short-term bidirectional IFT and diffusion and the newly imported complexes frequently replaced axoneme-bound ODAs. We propose that the low processivity of ODA-IFT contributes to flagellar maintenance by ensuring the availability of replacement ODAs along the length of flagella.**

Monitoring Editor
Thomas Surrey
The Francis Crick Institute

Received: May 11, 2018
Revised: Aug 1, 2018
Accepted: Aug 14, 2018

INTRODUCTION

Many protists propel and feed themselves by means of motile cilia. In mammals, mucociliary clearance of the airways, sperm locomotion, and establishing the correct left-right asymmetry of the body plan depend on ciliary motility (Nonaka *et al.*, 1998). Defects in ciliary motility cause primary ciliary dyskinesia, a genetically heterogeneous disorder characterized by chronic airway infections, situs anomalies including congenital heart defects, male infertility, and hydrocephalus and ventriculomegaly (Ibanez-Tallon *et al.*, 2004; Fliegauf *et al.*, 2007; Horani *et al.*, 2016; Mirra *et al.*, 2017). The bending of cilia requires the activity of axonemal dyneins, large multiprotein complexes that induce sliding between adjacent axonemal doublet microtubules (Satir, 1968; Goodenough and Heuser, 1982; Lin *et al.*, 2014). Most organisms with motile cilia possess both inner and outer dynein arms (IDAs and ODAs) with ODAs being the main force generator and controller of ciliary beat frequency (Brokaw, 1994; Desai *et al.*, 2015).

ODAs are complex machines consisting of three dynein heavy chains (HCs), two intermediate chains (ICs), and several light chains (Kamiya, 1988; King and Patel-King, 2015). They are preassembled in the cell body, transported as a holo complex into the cilium, and docked to the axonemal microtubules (Fowkes and Mitchell, 1998). Each of these steps is shepherded by one or more protein factors, which are not part of the mature ODAs (Desai *et al.*, 2018). *Kintoun/PF13/DNAAF2*, for example, is required for the preassembly of ODAs in the cell body (Omran *et al.*, 2008). A group of gene products (i.e., ODA5, ODA8, ODA10) appears to function as ODA maturation factors because ODAs are formed in mutant cytoplasm but are largely absent from flagella (Dean and Mitchell, 2013, 2015; Desai *et al.*, 2015).

This article was published online ahead of print in MBoC in Press (http://www.molbiolcell.org/cgi/doi/10.1091/mbc.E18-05-0291) on August 22, 2018.

The authors declare that they have no conflict of interest.

*Address correspondence to: Karl F. Lechtreck (lechtrek@uga.edu) or David R. Mitchell (mitcheld@upstate.edu).

Abbreviations used: BF, bright-field; HC, heavy chain; IC, intermediate chain; IFT, intraflagellar transport; NG, mNeonGreen; ODA, outer dynein arm; TIRF, total internal reflection fluorescence.

Once assembled, the ~2 MDa ODAs must move into flagella past a transition zone barrier that limits access by diffusion to proteins smaller than ~50 kDa (Kee *et al.*, 2012). Flagellar assembly and the transport of most axonemal proteins into flagella occur via intraflagellar transport (IFT; Kozminski *et al.*, 1993; Lechtreck, 2015). Trains of IFT particles, each consisting of 22 distinct proteins, move via molecular motors bidirectionally along the ciliary microtubules (Rosenbaum and Witman, 2002). Some proteins, for example, tubulin, interact directly with IFT trains, whereas the transport of other cargoes involves cargo adapters that mediate binding to the IFT train or stabilize the interaction (Bhogaraju *et al.*, 2013; Hunter *et al.*, 2018; Liu and Lechtreck, 2018). ODA16 is an ODA-specific IFT cargo adapter that interacts with the N-terminal region (i.e., head domain) of the IFT protein IFT46 (Ahmed and Mitchell, 2005; Ahmed *et al.*, 2008; Hou *et al.*, 2007; Gao *et al.*, 2010; Taschner *et al.*, 2017). Mutants expressing an N-terminally truncated IFT46 assemble cilia, albeit slowly, largely lacking ODAs but of otherwise normal ultrastructure (Hou *et al.*, 2007; Hou and Witman, 2017). ODA16 binds directly to ODAs in vitro, further supporting the notion that it mediates ODA-IFT interactions (Taschner *et al.*, 2017).

Once inside flagella, axonemal cargoes are released from IFT and bind to the axoneme. In *Chlamydomonas reinhardtii*, ODA binding to the axoneme involves a three-subunit docking complex (DC; Wakabayashi *et al.*, 2001; Ide *et al.*, 2013). Although the DC has been implicated in establishing the 24-nm repeat of ODA binding to doublets (Owa *et al.*, 2014), in vitro experiments show that ODAs still bind with a 24-nm periodicity to microtubules in the absence of the DC, suggesting that the primary role of the DC in vivo is to increase binding affinity (Oda *et al.*, 2016). ODAs are one of the most abundant axonemal proteins, other than tubulin, and are likely one of the largest axonemal complexes imported into cilia. Because IFT of ODAs has not yet been observed directly, it remains unknown how ODA transport and behavior are affected in the various mutants.

We expressed the essential ODA intermediate chain IC2 fused to mNeonGreen (NG) to rescue *oda6*, the corresponding *C. reinhardtii* mutant. Using single particle in vivo imaging, we formally demonstrate that ODAs are transported on IFT trains and analyze how their behavior inside flagella is affected in mutants with defects in ODA assembly, transport, and docking. In comparison to previously studied axonemal proteins, ODA transport was of lower processivity and retrograde transport was frequent, resulting in rapid mixing of soluble ODAs inside cilia. We noted a considerable rate of exchange of axonemal ODAs in full-length cilia and propose that these transport characteristics ensure rapid replacement of ODAs damaged during the lifetime of the axoneme.

RESULTS

IC2-NG largely rescues *oda6* mutants

To analyze the transport of ODAs in vivo, NG was fused to the C-terminus of the ODA subunit IC2 and expressed in *oda6* (Figure 1A). This mutant is unable to assemble ODAs due to the lack of functional IC2 and swims with reduced velocity (Figure 1, B and C). Western blot analysis of flagella isolated from control, mutant, and rescued strains with anti-IC2 identified a band of ~70 kDa in wild type (WT), which is absent in *oda6* flagella (Figure 1B). In the *oda6* IC2-NG strain, the endogenous IC2 was replaced by a band ~95 kDa representing IC2-NG; two additional faster migrating bands are likely to represent fragments of IC2-NG from premature termination. Expression of IC2-NG in *oda6* restored wild-type swimming velocity (Figure 1C). In vivo imaging revealed that IC2-NG is present in essence along the entire length of the flagella (Figure 1D). After photobleaching of IC2-NG in a flagellar segment, the bleached region did not recover within the time of the experiment (~1 min), indicating that most IC2-NG is stably anchored to the axoneme (Figure 1E). Already in the cell body, IC2 is embedded in a complex with other ODA subunits including the HCs (Fowkes and Mitchell, 1998). Further, IC2 is largely absent from the flagella of mutants lacking other ODA subunits (e.g., *oda2* encoding the HCγ) suggesting that it is unable to assemble onto the axoneme on its own (Fowkes and Mitchell, 1998). In conclusion, most IC2-NG present in the flagella of the rescue strain is likely to be incorporated into ODAs making IC2-NG a suitable reporter to study ODA transport in living cells.

IC2-NG is transported by IFT

To visualize individual IC2-NG particles moving inside flagella, we either photobleached IC2-NG already incorporated into the *oda6* axonemes or employed an *oda3 oda6* IC2-NG strain; the latter lacks the DC, preventing IC2-NG accumulation inside flagella (Figure 2 and Supplemental Figure S1; see below for a full description of IC2-NG behavior in *oda3* flagella). IC2-NG moved in both anterograde (from the base to the tip) and retrograde (from the tip to the base) directions along the flagella with velocities typical for IFT; the average velocities were 2.19 μm/s (SD 0.39 μm/s, $n = 136$) and 3.0 μm/s (SD 0.78 μm/s, $n = 89$) for anterograde and retrograde transports, respectively (Figure 2A and Supplemental Video S1). Using simultaneous two-color imaging in a strain expressing IC2-NG and the IFT-B protein IFT20-mCherry (mC) in the corresponding *oda6 ift20* double or *oda3 oda6 ift20* triple mutant, we confirmed that IC2-NG comigrates with IFT20-mC (Figure 2B and Supplemental Video S2). Frequently, IC2-NG separated from moving IFT20-mC trains before reaching the flagellar tip (Figure 2B). In the *oda6* IC2-NG single rescue strain, only 29% of IC2-NG transports move in one run from the base to the flagellar tip ($n = 86$ transports; Figure 2C). IC2-NG diffusing inside the flagellum frequently reassociated with moving IFT trains (Figure 2, A and B, and Supplemental Figure S1).

The transport frequency of several axonemal precursors is upregulated while cilia grow (Wren *et al.*, 2013; Craft *et al.*, 2015). To test whether the frequency of ODA transport is similarly regulated, we removed the flagella of *oda6* IC2-NG cells by a pH shock and allowed the cells to regenerate flagella for >20 min before live imaging (Figure 2D). The frequency of anterograde IC2-NG transport in photobleached regenerating *oda6* IC2-NG flagella was significantly elevated in comparison to that observed in full-length flagella (5.90 vs. 0.77 transports/min; Figure 2E). The observed maximum frequency in growing flagella was 27 anterograde IC2-NG transports/min. A single 12-μm-long *C. reinhardtii* flagellum contains ~4000 ODAs and is assembled over a period of ~90 min, resulting in a predicted frequency of ~45 ODA transports/min (Rosenbaum *et al.*, 1969). Thus, the transport frequency observed in vivo corresponds to just ~13% of the expected frequency. The difference between the predicted and experimental frequency can be explained at least in part by the observations that 1) some IFT trains carry two or more IC2-NG particles (Supplemental Figure S1C and Supplemental Video S3), 2) in some experiments, the levels of IC2-NG in flagella of the rescue strain were below that of endogenous IC2 in controls (unpublished data), 3) weaker trajectories likely escaped detection in regenerating cilia, and 4) some ODAs might enter cilia by diffusion (see below). In the case of the axonemal protein DRC4, the observed average transport frequency of its GFP-tagged derivative in growing flagella accounts for ~70% of the molecules needed in a full-length flagellum. It is also possible that the transport of certain cargoes is sensitive to immobilization and imaging of the cells. To summarize, ODAs as visualized by IC2-NG are transported by IFT, the transport

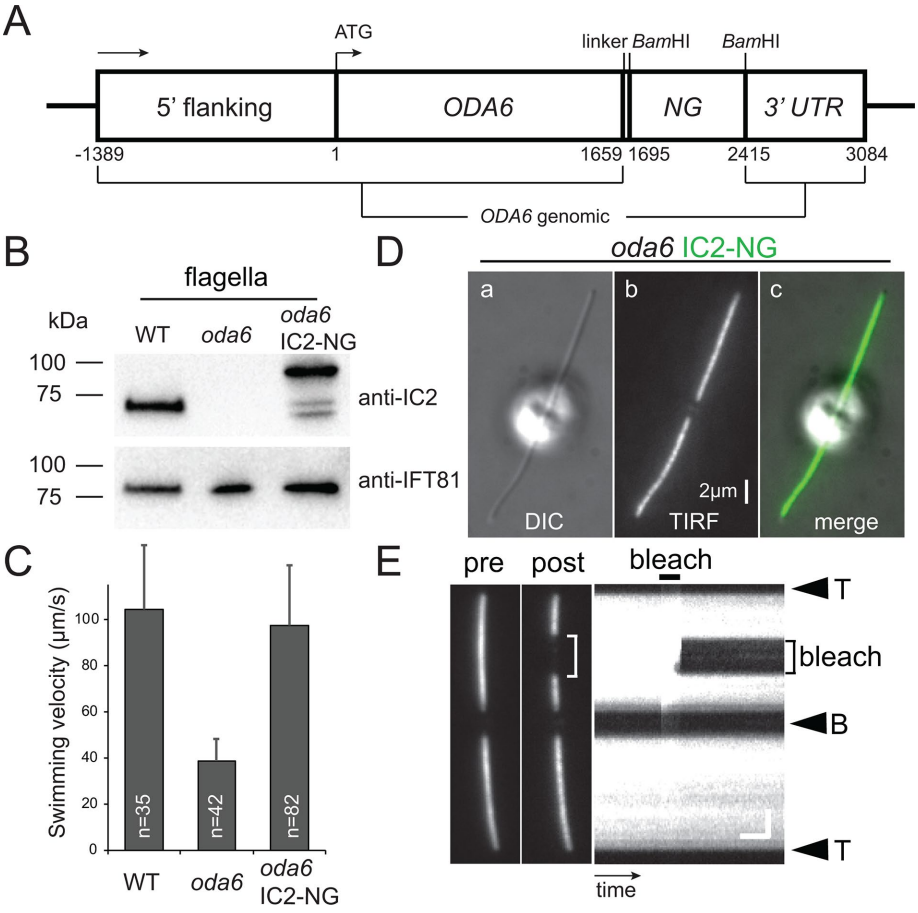

FIGURE 1: IC2-NG rescues the *oda6* mutant. (A) Schematic presentation of the IC2-NG expression vector. The sequence for NG was inserted at the 3′ end of the genomic *ODA6* coding region. (B) Western blot of isolated flagella from wild type, the *oda6* mutant, and the *oda6* IC2-NG rescue strain probed with antibodies against IC2 and IFT81 as a loading control. (C) Mean swimming velocity of wild type, *oda6*, and *oda6* IC2-NG strains. Error bars represent SD. *n*, number of cells analyzed. (D) Differential interference contrast (DIC) (a), TIRF (b), and the corresponding merged image (c) of a live *oda6* IC2-NG cell. Bar = 2 µm. (E) TIRF image of a live *oda6* IC2-NG cell before and ~10 s after bleaching of a flagellar segment, and the corresponding kymogram. The experiment demonstrates that most IC2-NG is stably anchored in the flagellum. The flagellar tip (T) and base (B) are indicated. Bars = 2 µm and 2 s.

is of comparatively low processivity, and the frequency of ODA transport is up-regulated during flagellar growth.

ODA assembly during flagellar repair

In quadriflagellate zygotes obtained by mating *C. reinhardtii* motility mutants to wild-type cells, the defects in the mutant-derived flagella are often repaired using protein encoded by the wild-type gene and stockpiled in the wild-type cytoplasm, which after cell fusion becomes available for transport into the mutant-derived flagella (Kamiya, 1988; Johnson and Rosenbaum, 1992; Dutcher, 2014). During the repair, most axonemal proteins are transported by IFT to the flagellar tip, where they are released; they then diffuse into the flagellar shaft and dock to the axoneme, filling up the docking sites closest to the tip first (Qin *et al.*, 2004; Wren *et al.*, 2013). Such a tip-to-base repair pattern has been observed for inner dynein arms (Piperno *et al.*, 1996; Viswanadha *et al.*, 2014), radial spokes (Johnson and Rosenbaum, 1992; Lechtreck *et al.*, 2018), dynein regulatory complexes (DRCs; Bower *et al.*, 2013; Wren *et al.*, 2013), and central pair projections (Lechtreck *et al.*, 2013). ODAs, however, are added concurrently along the entire length of *oda6*-derived flagella in similar dikaryon rescue experiments (Piperno *et al.*, 1996). To test how this repair pattern correlates with the distribution of ODA unloading sites from IFT, we mated *oda6* to *oda6* IC2-NG gametes and analyzed the resulting zygotes by total internal reflection fluorescence (TIRF) microscopy (Figure 3A). As previously reported based on antibody staining, IC2-NG addition occurred simultaneously along the length of *oda6*-derived acceptor flagella (Figure 3B). During the repair of *oda3 oda6* double mutant acceptor flagella, in which the assembly of the missing DC has to precede the binding of the ODAs, the addition of IC2-NG progressed largely from the base to the tip as previously reported (Figure 3B; Wakabayashi *et al.*, 2001). Thus, IC2-NG recapitulates the behavior of untagged IC2 during the repair of mutant flagella. After photobleaching all four flagella of *oda6* IC2-NG × *oda6* zygotes, individual transports became visible (Figure 3C). Just as in the cilia of vegetative cells, IC2-NG detached from IFT at various sites along the zygotic acceptor and donor flagella (Figure 3C). In *oda6*-derived flagella, most IC2-NG particles instantaneously became stationary after unloading from IFT, indicative of docking to unoccupied sites on the axoneme (Figure 3C and Supplemental Video S4). When unloaded inside the *oda6* IC2-NG–derived donor flagella, in which the ODA docking sites are occupied, IC2-NG diffused, reloaded onto anterograde or retrograde IFT, and only occasionally became stationary (Figure 3C). Compared to other cargoes, retrograde IFT of IC2-NG is more frequent, ensuring a redistribution of unloaded ODAs toward the flagellar base (Figure 2E). In conclusion, premature unloading from IFT trains at various sites along the flagellum and frequent retrograde transport likely explain IC2-NG incorporation concurrently along the length of mutant-derived flagella.

We wondered whether cells adjust the transport frequency of IC2-NG in response to demand, that is, the absence of ODAs from flagella. In *oda6* × *oda6* IC2-NG zygotes, the average number of anterograde transports was 3.82/min in the *oda6*-derived flagella and 5.07/min in the *oda6* IC2-NG derived flagella (Figure 3D). These values were not significantly different from the average transport frequency of IC2-NG in the four flagella of WT × *oda6* IC2-NG zygotes (4.05/min and 3.96/min for WT and *oda6* IC2-NG–derived flagella, respectively; Figure 3D). We assume that IC2-NG will eventually exit flagella that lack docking sites via either diffusion or IFT. The data indicate that cells do not adjust the frequency of ODA transport in response to ODA deficiency.

Zygotes formed by mating of *oda6* IC2-NG to wild-type gametes allowed us to assess the exchange of ODAs by monitoring the incorporation of IC2-NG into the wild-type derived flagella.

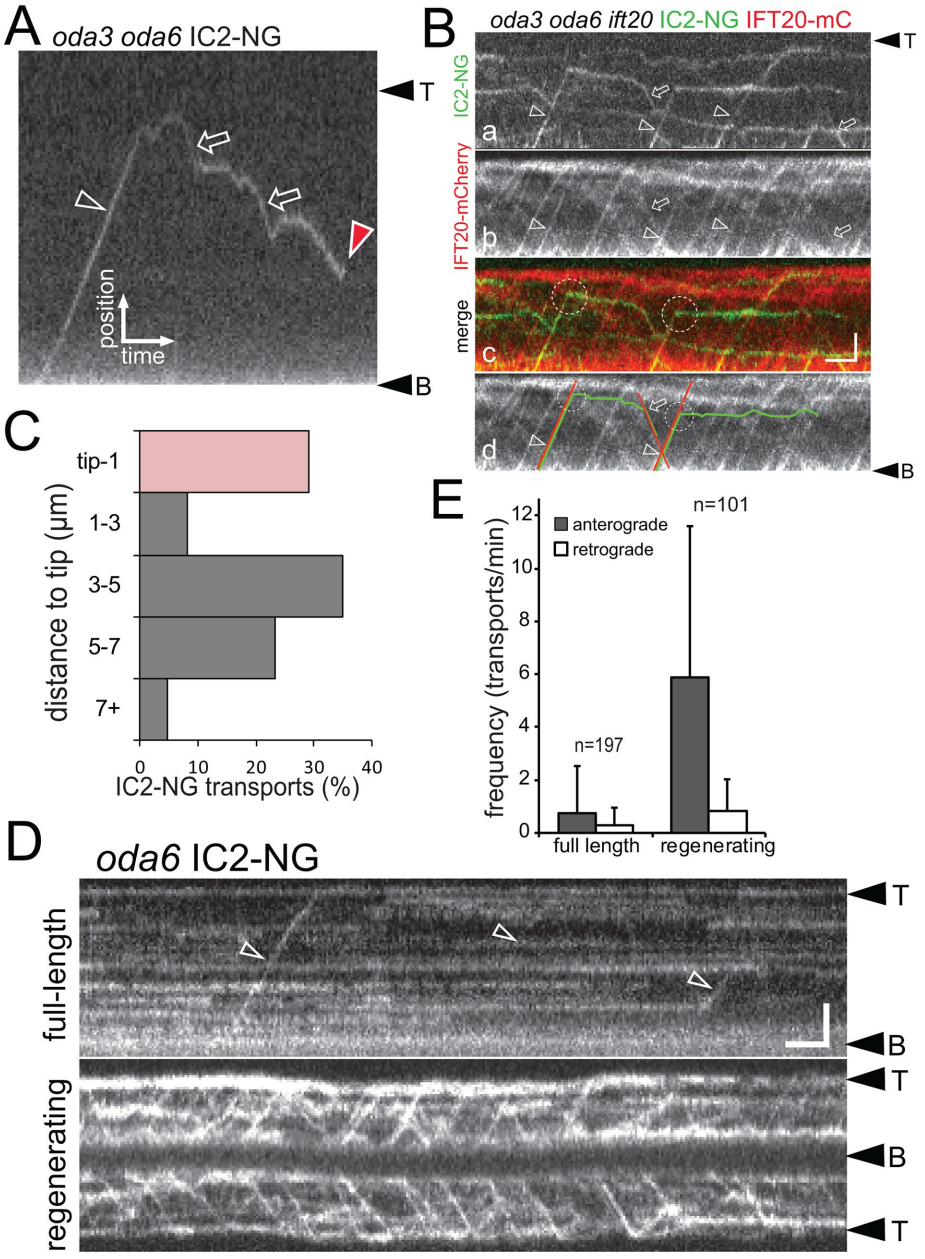

FIGURE 2: IC2-NG is transported by IFT. (A) Kymogram showing anterograde (open arrowhead) and retrograde (open arrows) transport of IC2-NG in full-length *oda3 oda6* flagella. Red arrowhead, one-step bleaching of the IC2-NG particle indicative for a single NG protein. Bars = 2 µm and 2 s. (B) Kymograms showing simultaneous two-color imaging of IC2-NG (a) and IFT20-mCherry (b) in *oda3 oda6 ift20* flagella. A merged imaging is shown in c, and the trajectories of two transports are marked in d. Arrowheads and arrows mark anterograde and retrograde cotransport of IC2-NG and IFT20-mCherry; dashed circles indicate unloading of IC2-NG. Bars = 2 µm and 2 s. (C) Distribution of IC2-NG unloading from anterograde IFT expressed in distance from the flagellar tip. (D) Kymograms depicting IC2-NG in fully grown (top) and regenerating (bottom) *oda6* flagella; flagella were partially photobleached before the recording. Open arrowheads, anterograde transports. Bars = 2 µm and 2 s. (E) The frequencies of anterograde and retrograde transport of IC2-NG in full-length and regenerating *oda6* flagella. Two-tailed *t* test resulted in $p < 0.0001$ for the frequencies of anterograde IC2-NG transport in full-length vs. regenerating flagella and a low significance score of $p = 0.051$ for the retrograde transport frequencies. Error bars indicate SD; *n*, number of cilia analyzed.

IC2-NG gradually appeared in a spotted distribution along wild-type–derived flagella often with stronger signals in the proximal regions. Kymograms revealed that many of these particles are stationary, indicating that they could result from an exchange of untagged ODAs with IC2-NG–containing ODAs (Figure 3E). Zygotes can form as early as <60 s after combining the gametes but often cell fusion requires more time. This heterogeneity prevents precise determination of the age of zygotes and the time course of ODA exchange. In zygotes imaged ~3 h after mixing of the gametes, the signal strength in the wild-type–derived cilia was on average 11% of that in the donor flagella (SD 4.8%, $n = 23$). Estimates of the exchange rate need to take into account that such zygotes possess both tagged and untagged IC2. Incorporation of untagged ODAs into the acceptor flagella will escape detection and incorporation into the donor flagella will reduce the IC2-NG reference signal used for quantification. On the basis of these considerations, we estimate that ~7% of the 4000 ODAs in a *C. reinhardtii* flagellum are exchanged per hour.

IFT and axonemal binding of IC2-NG are impaired in *oda2*

IC2 is largely absent or reduced in flagella of numerous mutants with defects in either other ODA subunits or proteins that are not subunits of the ODAs themselves but assist with ODA assembly, maturation, flagellar transport, and axonemal docking (Table 1). We used in vivo imaging of IC2-NG to elucidate how the different mutations affect the behavior of ODAs in flagella.

First, we generated an *oda2 oda6* IC2-NG strain to test the ability of IC2-containing ODA fragments to enter cilia and move by IFT (Figure 4). In *oda2*, the ODA HCγ is missing, whereas the βHC and the two ICs are present in the cytoplasm; the two ICs are in a complex but HCβ fails to coimmunoprecipitate with this complex (Fowkes and Mitchell, 1998). In vivo imaging showed IC2-NG diffusing inside *oda2* cilia; IFT of this complex was rare and docking was only observed near the flagellar base (Figure 4, A and B). After photobleaching, IC2-NG reentered *oda2* flagella by diffusion (Figure 4C). The diffusional mobility of a protein complex depends on its size. In control flagella, IC2-NG diffused slower than, for example, tagged EB1 or RSP4, in agreement with the large size of the ODAs (~2000 kDa; Supplemental Figure S2A). In *oda2* flagella, the diffusional mobility of IC2-NG was above that observed for intact ODAs in control flagella in agreement with the presence of a smaller IC2-NG containing complex (Supplemental Figure S2). In summary, the partial ODA complexes present in *oda2* flagella are essentially unable to interact with IFT or the axonemes.

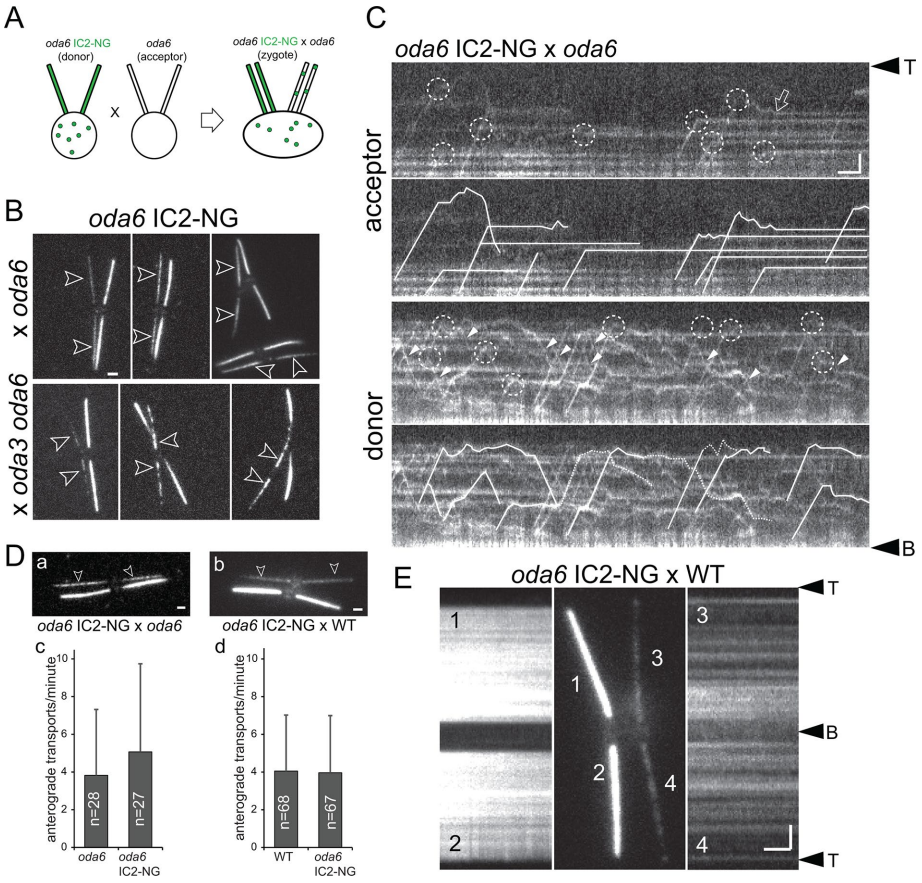

FIGURE 3: ODAs dock rapidly to the axoneme after unloading from IFT. (A) Schematic presentation of a dikaryon rescue experiment by mating donor gametes expressing IC2-NG (green) to *oda6* acceptor gametes lacking IC2 or IC2-NG. After cell fusion, IC2-NG present in the shared cytoplasm is available for transport into the mutant-derived flagella. (B) TIRF images of live zygotes from a mating between *oda6* IC2-NG with either the *oda6* single or *oda3 oda6* double mutant. IC2-NG is added simultaneously along *oda6* flagella and with a proximal–distal gradient in *oda3 oda6* flagella. Bar = 2 µm. (C) Kymograms of the acceptor and donor flagella of *oda6* × *oda6* IC2-NG zygotes; the flagella were photobleached to allow imaging of moving IC2-NG complexes. The kymograms are shown in duplicate: in the top panels, unloading events are marked by dashed circles; in the bottom panels, individual particles are traced (dashed lines indicate uncertainty). In the *oda6*-derived flagella, unloading is followed by docking as indicated by the lack of movement. Open arrow: IC2-NG docking event after a brief period of diffusion. Note frequent wide distribution of unloading sites along the length of the flagella, docking of IC2-NG in the acceptor flagella (top panels), and extended periods of diffusion and frequent retrograde IFT (closed arrowheads) of IC2-NG when unloaded in donor-cell–derived flagella with occupied docking sites (bottom panels). Bars = 2 µm and 2 s. (D) Still images (a,b) and anterograde transport frequency (c, d) of IC2-NG in flagella of *oda6* IC2-NG × *oda6* and *oda6* IC2-NG × WT zygotes. (E) TIRF images and corresponding kymograms of an *oda6* IC2-NG × WT zygote analyzed ~3.5 h after mixing of the gametes. Bar = 2 µm and 2 s.

ODAs are docking incompetent in oda8 and transport incompetent in *oda10*

Mutants in *ODA8* and *ODA10* assemble ODAs in the cytoplasm that apparently contain all subunits but the isolated complexes fail to decorate stripped wild-type axonemes (Fowkes and Mitchell, 1998; Desai *et al.*, 2018). In contrast, wild-type ODAs will bind to *oda8* and *oda10* axonemes in vitro, indicating that the docking sites are unaffected (Fowkes and Mitchell, 1998). Thus, ODAs preassembled in *oda8* and *oda10* are defective and ODA8 and ODA10 have been also referred to as ODA maturation factors (Dean and Mitchell, 2015). Biochemical studies, however, indicate distinct roles for each protein in flagella with ODA8 being mostly IFT associated, whereas ODA10 is bound to the axoneme.

The transport of IC2-NG was strongly reduced in both *oda10* flagella (or *oda10* × *oda10* zygotic flagella) and especially in *oda8* flagella (or *oda8* × *oda8* zygotic flagella) and only a few IFT-based transports were observed during this study (Figure 5). In *oda10*, most IC2-NGs observed were docked to the axoneme and diffusing IC2-NG apparently became quickly stationary preferably in the distal segment of *oda10* flagella (Figure 5A). In contrast, IC2-NG was mostly diffusing for extended periods in *oda8* flagella without associating with either IFT or the axoneme (Figure 5B and Supplemental Video S5). Of note, the diffusional mobility of IC2-NG in *oda8* flagella was variable; the presence of both full-size and partial ODAs in mutant flagella could explain this observation (Supplemental Figure S2B). The data suggest that IFT of ODA is largely impaired in *oda10;* however, those ODAs that enter the flagellum by diffusion and residual IFT dock normally. In contrast, the behavior of IC2-NG in *oda8* flagella indicates a defect in docking in addition to possible defects in ODA IFT and assembly.

Residual entry of IC2-NG into *oda16* and *ift46* IFT46ΔN flagella

Previous studies identified ODA16 as an IFT-associated protein essential for efficient ODA assembly (Ahmed and Mitchell, 2005). ODAs isolated from *oda16* cytoplasm bind to *oda16* axonemes indicating that the mutation affects ODA transport (Ahmed *et al.*, 2008). ODA16 binds both ODAs and the N-terminal domain of IFT46, and cells lacking the head domain of IFT46 (*ift46 IFT46ΔN*) also assemble flagella largely lacking ODAs (Hou and Witman, 2017; Taschner *et al.*, 2017), consistent with the model that ODA16 is a cargo adapter ensuring ODA transport by IFT.

IFT of IC2-NG was observed only sporadically in *oda16* and *ift46 IFT46ΔN* flagella, confirming the importance of ODA16 and IFT46 for ODA transport (Figure 6, A–D). Despite the near lack of ODA transport, significant amounts of IC2-NG are incorporated into *ift46 IFT46ΔN* and especially *oda16* flagella (Figure 6, A and C, and Supplemental Figure S3E; Ahmed and Mitchell, 2005; Hou and Witman, 2017). The distribution of IC2-NG in the mutant flagella was somewhat variable between individual cells of the same strain. In most *ift46 IFT46ΔN* cells analyzed, IC2-NG was largely restricted to the proximal flagellum and the signal tapered toward the flagellar tip (Figure 6B and Supplemental Figure S3C). In *oda16*, IC2-NG was typically restricted to a middle segment of the flagellum often with clear-cut edges

Strain	Protein encoded by wild-type gene	Complex/ process	Amount in flagella	Transport by IFT	Axonemal binding	Presence at base
oda6 IC2-NG (control)			+++	+++	+++	+
oda2 oda6 IC2-NG	HCγ	ODA subunit	(+)	(+)	–	–
oda3 oda6 IC2-NG	DC1	docking complex	(+)	+++	–*	+
oda8 oda6 IC2-NG	ODA8	ODA maturation	(+)	+	(+)	(+)
oda10 oda6 IC2-NG	ODA10	ODA maturation	+	(+)	+	n.d.
oda16 oda6 IC2-NG	ODA16	ODA transport	++	(+)	+++	(+)
ift46 IFT46ΔN oda6 IC2-NG	IFT46	ODA transport	+	(+)	+++	+++
oda16 ift46 IFT46ΔN oda6 IC2-NG	ODA16 IFT46	ODA transport	+	(+)	+++	–

+++, frequent; +, infrequent; (+), rarely observed; –, not observed; *transient docking was observed; n.d., not determined.

TABLE 1: Overview of the strains used and the observed defects in cilia entry, IFT, and axonemal binding of IC2-NG.

(Figure 6A and Supplemental Figure S3, A and B). In regenerating *oda16* flagella, however, IC2-NG typically accumulated near the flagellar base mimicking the distribution in the *ift46 IFT46ΔN* background (Supplemental Figure S3B). In both strains, the signal was often more spread out when flagella contained only little IC2-NG putatively indicating a dose-dependent cooperativity in ODA clustering. To further explore the differences in the distribution of residual IC2-NG in mutant flagella, we generated an *oda16 ift46 IFT46ΔN oda6* IC2-NG strain (Figure 6E). IFT of IC2-NG was rare but still observed in this quintuple mutant (unpublished data) and IC2-NG still accumulated in the proximal regions of the flagella reminiscent of IC2-NG in the *ift46 IFT46ΔN oda6* mutant (Figure 6F and Supplemental Figure S3, D and E). After photobleaching, IC2-NG reentered *oda16* and *ift46 IFT46ΔN* flagella by residual IFT and apparently by diffusion, likely explaining the partial presence of ODAs in *oda16* and *ift46 IFT46ΔN* flagella (Figure 6, G and H).

ODA16-dependent accumulation of IC2-NG near the basal bodies

Using a steeper TIRF angle to image deeper into the cell body, IC2-NG was observed in two small regions neighboring the two basal bodies in most (20 of 25 cells analyzed; Supplemental Figure S3F) vegetative wild-type cells; the signals were similar in cells with full-length and growing flagella (Figure 7A). In gametes and zygotes, however, each flagellum-bearing basal body was associated with two such IC2-NG signals. Two IC2-NG dots total were also present in most *oda3* cells while the signals were absent or largely absent in *oda2*, *oda8*, and *oda16* (Supplemental Figure S3F). Interestingly, prominent accumulations of IC2-NG were observed near the basal bodies of the *ift46 IFT46ΔN* cells (32 of 35 cells; Figure 7A). In *oda16 ift46 IFT46ΔN oda6* mutants, the IC2-NG signals at the flagellar base were diminished or absent suggesting that IC2-NG accumulation near the basal bodies requires ODA16. Similarly, the IC2-NG signals were weak or absent in *oda8 ift46 IFT46ΔN oda6* mutants (absent in 19 of 29 cells), suggesting that only intact ODAs can accumulate near the basal bodies. The IC2-NG buildups in *ift46 IFT46ΔN* were variable in intensity and size but often resembled two V-shaped to one large X-shaped signal (Figure 7A). This distribution suggests that IC2-NG is present along the proximal portions of the four cruciate microtubular roots (Ringo, 1967). After photobleaching of parts of IC2-NG signal with a focused laser beam, the bleach region recovered in ~9.8 s (SD 4.2 s, $n = 12$); prebleach intensity, however, was not reached and the intensity of the unbleached signal decreased, revealing that IC2-NG in the basal body–associated pool is not static, suggesting that ODAs rapidly exchange within the pool (Figure 7B).

Immunostaining of methanol-fixed cells was used to further analyze how mutations in *ODA16* and *IFT46* affect the distribution of IC2-NG. In control cells, antibodies to IC2 stained the flagella, the basal body region, and weak signals extending from the flagellar base down into the cell body; the antibodies to ODA16 strongly stained the

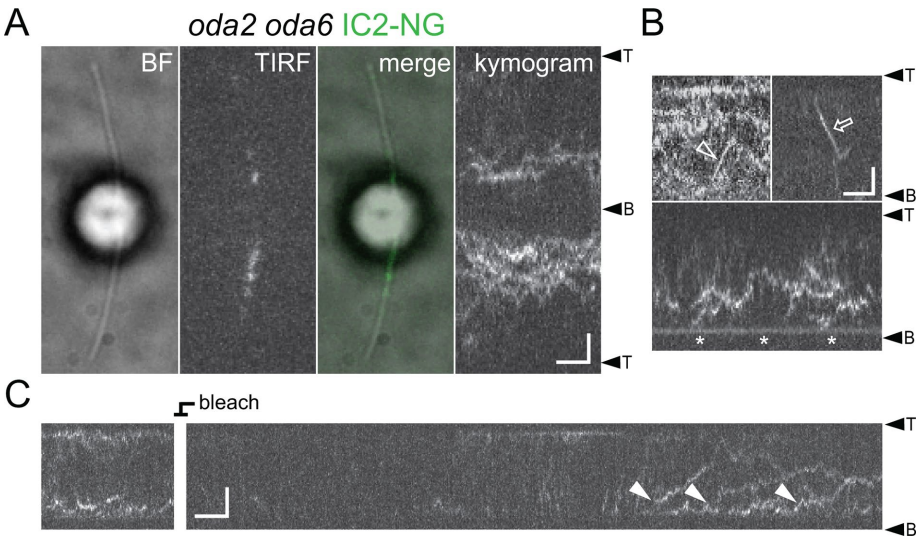

FIGURE 4: IFT and axonemal docking of IC2-NG is diminished in *oda2*. (A) Bright-field (BF), TIRF and merged image, and the corresponding kymogram of an *oda2 oda6* IC2-NG cell. Bars = 2 µm and 2 s. (B) Gallery of kymograms showing IFT (open arrow and arrowhead) and docking near the flagellar base (asterisk) of IC2-NG in *oda2* flagella. Bars = 2 µm and 2 s. (C) Kymogram showing incompletely assembled ODA containing IC2-NG diffusing into the *oda2* flagellum (closed arrowheads). The IC2-NG signals inside the flagellum were first photobleached to distinguish new entry events. Bars = 2 µm and 2 s.

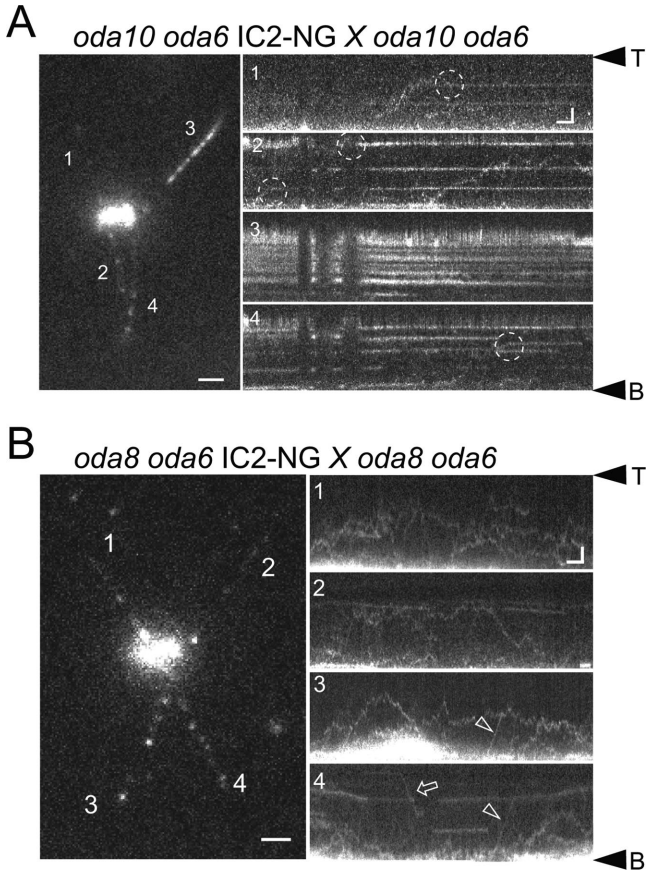

FIGURE 5: Transport and axonemal docking of ODAs are impaired in *oda8*. (A) Still image (four-frame average) and kymograms (1–4) of an *oda10 oda6* × *oda10 oda6* IC2-NG zygote. The kymograms are numbered correspondingly to the flagella in the still image. Dashed circle, putative docking event. Bars = 2 µm and 2 s. (B) Still image and kymograms of an *oda8 oda6* × *oda8 oda6* IC2-NG zygote. Bars = 2 µm and 2 s. Anterograde (arrowheads) and retrograde (arrows) IFT are marked. Note extended diffusion of ODAs in *oda8* while most ODAs are stationary in *oda10*.

flagellar base and weakly regions elsewhere in the cell (Figure 7C). These signals were essentially absent in the corresponding *oda6* and *oda16* mutants confirming the specificity of the antibodies (King and Witman, 1990; Ahmed *et al.*, 2008). Immunostaining of *ift46 IFT46ΔN* cells confirmed the accumulation of IC2-NG in the basal body region; the signal at the flagellar base was diminished in the absence of ODA16 in both the *oda6* IC2-NG and the *oda6* IC2-NG *ift46 IFT46ΔN* backgrounds. In these three transport mutants, IC2-NG strongly accumulated deeper inside the cell. These foci of IC2-NG might be related to the recently reported dynein preassembly complexes (Horani *et al.*, 2018). The data suggest that IC2-NG is recruited to the basal bodies in an ODA16-dependent manner; a failure to exit the pool via IFT due to the loss of the IFT46 head domain could result in a buildup of IC2-NG near the basal bodies.

IC2-NG transiently docks to *oda3* axonemes

Assembly of ODAs onto the axoneme requires the DC, a three-subunit particle consisting of DC1 (encoded by *oda3*), DC2, and DC3 (Koutoulis *et al.*, 1997; Casey *et al.*, 2003). In *oda3*, ODAs are largely absent from flagella in vivo but are thought to be structurally and functionally intact (Takada *et al.*, 1992). To study the behavior of ODAs in the absence of stable binding, we generated a strain expressing IC2-NG in the *oda3 oda6* double mutant background (Figure 8 and Supplemental Figure S1). For our analysis, we also used *oda3 oda6* × *oda3 oda6* IC2-NG zygotes (Figure 8A). In *oda3* flagella, IC2-NG transitioned frequently between anterograde and retrograde IFT, diffusion, and transient stationary phases; diffusion was slow, similar to that of IC2-NG in wild-type flagella (Figure 8A, Supplemental Figure S2, and Supplemental Video S6). Transient docking of IC2-NG lasted on average 4 s (SD 3.92 s, $n = 69$; Figure 8, B and C). Two-color imaging confirmed that IC2-NG dissociates from moving IFT trains at the onset of diffusion and was not associated with pausing IFT trains while being stationary along the flagellum (Supplemental Figure S1A; Stepanek and Pigino, 2016). Thus, ODAs still bind to axonemes in the absence of intact DCs but the association is unstable. In Supplemental Figure S4, we compiled kymograms of wild-type and various mutant flagella allowing for a side-by-side comparison of IC2-NG behavior.

DISCUSSION

IC2-NG is a cargo of IFT

In 1996, Piperno and coworkers suggested that ODAs move to their axonemal docking sites by an IFT-independent mechanism (Piperno *et al.*, 1996). However, the number of ODAs entering flagella is strongly reduced in the *oda16* and *ift46 IFT46ΔN* mutants (Hou *et al.*, 2007; Ahmed *et al.*, 2008). The former lacks the IFT-associated protein ODA16, which binds to ODAs, and the latter lacks the head domain of IFT46, which interacts with ODA16 (Taschner *et al.*, 2017). Together, these data strongly indicate that IFT participates in the delivery of ODAs into cilia. Here, we show that the essential ODA subunit IC2-NG moves on IFT trains in flagella and that the transport frequency is strongly reduced in the absence of intact ODA16 or the head domain of IFT46. Thus, ODAs are cargoes of IFT. Incomplete inhibition of IFT or residual entry of ODAs by diffusion could explain the assembly of ODAs observed in flagella of zygotes expressing the fast-acting *fla10-1* allele, which inhibits IFT at the nonpermissive temperature (Piperno *et al.*, 1996).

IFT and docking of ODAs are defective in oda8

In vivo imaging of IC2-NG provides a visual manifestation of how ODA behavior inside cilia is affected in mutants with defects in ODA assembly, maturation, transport, and axonemal docking. In *oda8*, for example, IC2-NG mostly diffused inside flagella with a mobility above that observed in wild type and *oda3* and both transport and axonemal binding were strongly impaired supporting the notion that *oda8* ODAs are defective and largely unable to bind to either IFT trains or the axoneme. Because *oda8* ODAs isolated from the cell body are thought to contain all known ODA subunits (Desai *et al.*, 2015), the defects could be caused by changes in the configuration of the complex. Also, the identification of complete ODAs in *oda8* does not exclude the presence of smaller complexes that might diffuse into flagella. The low mobility of IC2-NG complexes observed in wild-type flagella could also result from ODAs diffusing in weak association along the microtubules, a behavior that has been described for several other proteins (Zimmermann *et al.*, 2011; Hinrichs *et al.*, 2012). Then, the increased mobility of IC2-NG in *oda8* could result from impaired microtubule interaction of the ODAs, in agreement with the observed defects in axonemal binding of *oda8* ODAs. It is interesting to speculate whether the *oda8* mutation affects two independent binding sites, one for IFT and one for the axoneme, or whether these two sites are actually overlapping. The latter would prevent binding of ODAs to the axoneme while moving on IFT trains and would be consistent with the evolutionary relationship between the DC1/DC2 heterodimer in the docking

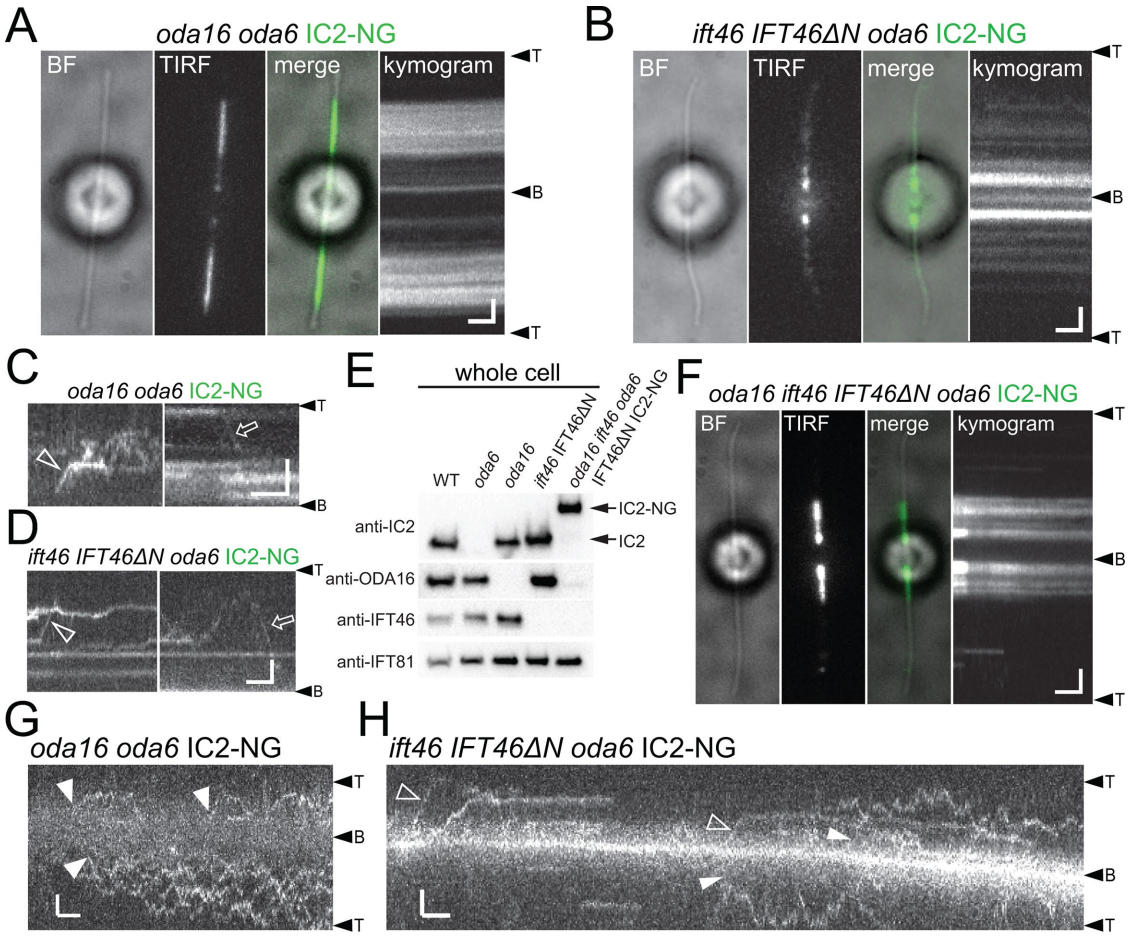

FIGURE 6: Distinct distribution of IC2-NG in *oda16* and *ift46 IFT46ΔN* flagella. (A) BF and TIRF image and the corresponding kymogram of a live *oda16 oda6* IC2-NG cell. (B) BF and TIRF image and the corresponding kymogram of a live *ift46 IFT46ΔN oda6* IC2-NG cell. (C) Gallery of kymograms showing sporadic IFT (open arrow and arrowhead) of IC2-NG in *oda16 oda6* IC2-NG flagella. (D) Gallery of kymograms showing sporadic IFT (open arrow and arrowhead) of IC2-NG in *ift46 IFT46ΔN oda6* IC2-NG flagella. Bars (A–D) = 2 µm and 2 s. (E) Western blot analysis of whole cell extracts from the strains indicated documenting the generation of the *oda16 ift46 oda6 IFT46ΔN* IC2-NG quintuple strain. Note that the antibody raised against the head domain of IFT46 will not react with *IFT46ΔN*. (F) BF and TIRF image and the corresponding kymogram of a live *oda16 ift46 oda6 IFT46ΔN* IC2-NG cell. Bars = 2 µm and 2 s. (G) Kymograms showing the entry of IC2-NG into photobleached *oda16 oda6* IC2-NG flagella by apparent diffusion (closed arrowheads). Bars = 2 µm and 2 s. (H) Kymograms showing the entry of IC2-NG into photobleached *ift46 IFT46ΔN oda6* IC2-NG flagella by IFT (open arrowheads) and apparent diffusion (closed arrowheads). Bars = 2 µm and 2 s.

complex and the ODA5/ODA10 heterodimer involved in ODA trafficking (Dean and Mitchell, 2015). A binding site on the ODA complex that is occupied with the ODA5/ODA10 dimer during late stages of assembly and transport could associate with the docking complex after ODA release from IFT. Although DRC4-GFP released from IFT typically diffuses for several seconds before docking to the axoneme, ODA docking occurred mostly instantaneously upon release from IFT; brief phases of diffusion were observed when unloading occurred in regions where most docking sites were already occupied. Similarly, the transition from IFT to transient docking and vice versa in *oda3* flagella often occurred directly without noticeable diffusion in between. This pattern suggests that a high-affinity axonemal binding site of the ODAs might be hidden while they are bound to IFT trains. In contrast to *oda8*, most ODAs in the flagella of the *oda10* mutant were docked to the axoneme but IFT was observed only occasionally, suggesting that the lack of ODAs in this mutant is caused by a defect in ODA assembly or transport rather than docking.

ODA16 and IFT46 are required for effective IFT of ODAs

As expected, IC2-NG transport was largely abolished in *oda16* and *ift46 IFT46ΔN*. In the mutant and the double mutant, residual IFT of IC2-NG was observed, suggesting that neither ODA16 nor the head domain of IFT46 is absolutely essential for ODA–IFT interaction. Potentially, other regions of the IFT train or particle contribute to ODA binding allowing for sporadic transports. In agreement with previous data, *oda16* flagella possessed considerably more IC2-NG than *ift46 IFT46ΔN* flagella, suggesting that the IFT46 head domain is more critical for ODA transport than ODA16 (Hou and Witman, 2017). Surprisingly, IC2-NG was more abundant in the *oda16 ift46 IFT46ΔN* double than in the *ift46 IFT46ΔN* single mutant. ODA16 near the basal bodies could capture ODAs reducing its diffusional entry into flagella in situations when regular transport is impaired. Thus, it seems possible that ODAs, despite their large size, can pass through the diffusion barrier of the transition zone in agreement with reports showing entry of proteins of ~650 kDa into cilia by diffusion (Kee *et al.*, 2012; Lin *et al.*, 2013).

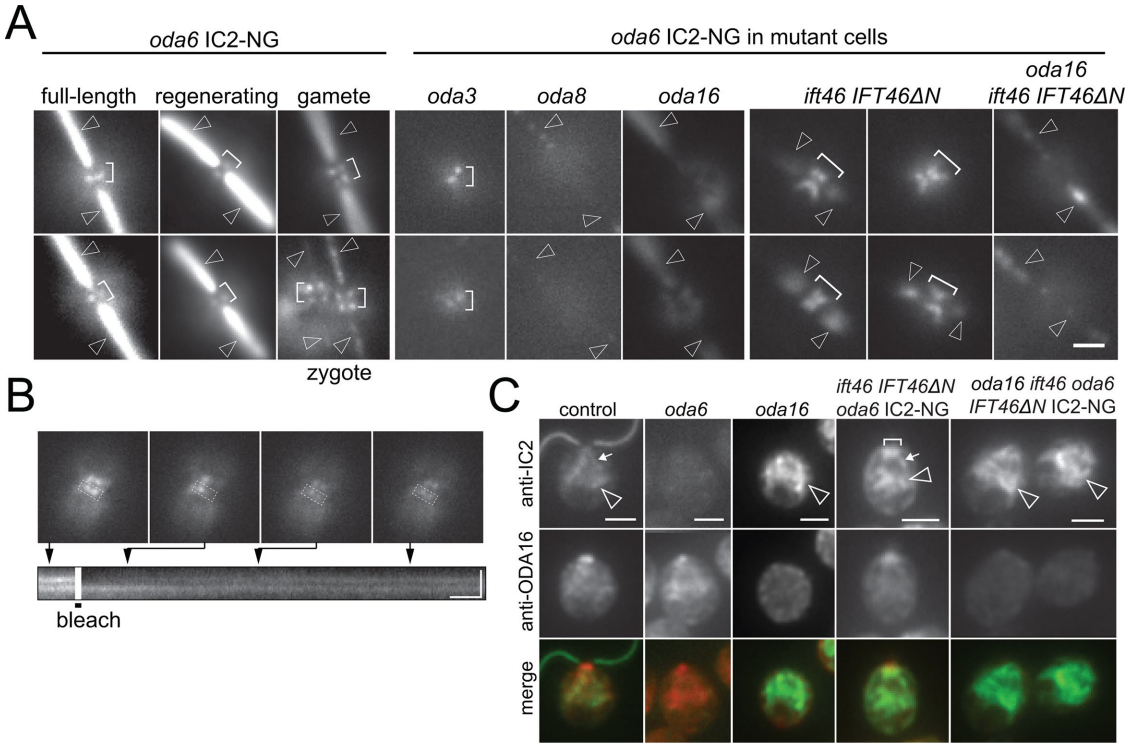

FIGURE 7: ODA16-dependent recruitment of IC2-NG to the flagellar basal bodies. (A) Image gallery showing IC2-NG at the flagellar base. Note that the signals are offset from the axis of the two flagella suggesting a position adjacent to the flagella-bearing basal bodies. Shown are IC2-NG in *oda6* cells with regenerating and full-length flagella and in gametes, in *oda6* × WT zygotes, in *oda3 oda6*, *oda8 oda6*, *oda16 oda6*, *ift46 IFT46ΔN oda6*, and *oda16 ift46 IFT46ΔN oda6* cells. Brackets, IC2-NG signals near the basal bodies; arrowheads, flagella. Bar = 2 µm. (B) Fluorescence recovery after photobleaching analysis of IC2-NG near the basal bodies in an *ift46 IFT46ΔN oda6* IC2-NG cell. Top: Still images of the cell before and after bleach of a portion of the IC2-NG pool and during recovery of the signal. Bottom: Kymogram corresponding to the boxed area showing signal recovery. Bars = 2 µm and 2 s. (C) Gallery of methanol-fixed cells of the strains indicated stained with antibodies to IC2 and ODA16; merged images are shown in the bottom row. Bracket, IC2-NG accumulation near the basal bodies; small arrow, elongated root-like signals of IC2-NG; arrowheads, accumulations of IC2-NG in the cell body. Bar = 2 µm.

Considering the continuous influx of ODAs into *oda16* and *ift46 IFT46ΔN* flagella by diffusion and residual IFT, it is unclear why more ODAs are not assembled into the mutant flagella over time. It seems possible that ODA docking or the DC are also affected in *oda16* and *ift46 IFT46ΔN*, which likely reflects differences in the distribution of the DC, the amount of which is reduced in *oda16* mutant flagella (Ahmed *et al.*, 2008; Hou and Witman, 2017). Also, the DC progressively fails to assemble toward the flagellar tip in the absence of ODAs suggesting an interdependence of ODA and DC assembly (Wakabayashi *et al.*, 2001). Because residual DC is preferably present near the flagellar base, ODA entry by diffusion and docking to nearby sites could explain the proximodistal gradient of ODAs observed in *ift46 IFT46ΔN* flagella. Additionally, if axonemal ODAs continually turn over, then the entry rate of new ODAs into the mutant cilia may not be enough to compensate the rate of turnover, resulting in incomplete site occupancy.

ODAs accumulate at the flagellar base when entry into the flagellum is impaired

In all three transport mutants (*oda16*, *ift46 IFT46ΔN*, and *oda16 ift46 IFT46ΔN*), substantial amounts of IC2-NG accumulated deep inside the cell body potentially demarking the sites of ODA storage or production. Recent studies in multiciliated cells have identified droplet-like structures as the sites of ODA assembly (Horani *et al.*, 2018). Additionally, IC2-NG accumulated near the flagellar base in the *ift46 IFT46ΔN* mutant. In wild-type control cells, only small foci of IC2-NG were present near each flagella-bearing basal body. The loading of cargoes onto IFT trains is thought to occur at the flagellar base (Wren *et al.*, 2013; Wingfield *et al.*, 2017). Because ODA transport is largely abolished in *ift46 IFT46ΔN*, ODAs destined for transport could build up at the flagella base. The IC2-NG signal near the basal bodies was weak and often absent in the *oda16* and *oda16 ift46 IFT46ΔN* mutants suggesting that ODA16 is required to recruit IC2-NG to the flagellar base, in addition to its function in ODA transport. In *oda3*, IC2-NG IFT occurred normally and wild-type–like IC2-NG signals were observed near the basal bodies indicating that a failure to assemble ODAs quantitatively into the axoneme is not sufficient to induce ODA accumulation near the basal bodies. We propose that ODA loading onto IFT is a two-step process, in which intact ODAs are recruited to the flagellar base in an ODA16-dependent manner and then handed over to IFT trains. Recruitment to the base largely failed in *oda2*, expressing only an ODA subcomplex, and in *oda8*, in which ODAs are transport and docking incompetent, suggesting that only intact ODAs are recruited to the flagellar base. Such a quality control mechanism at the flagellar base has been also suggested for tubulin (Stephan *et al.*, 2007).

The DC stabilizes ODA–axoneme interaction in vivo

The docking complex is thought to establish the 24-nm repeat of ODAs along the axonemal microtubules (Wakabayashi *et al.*, 2001;

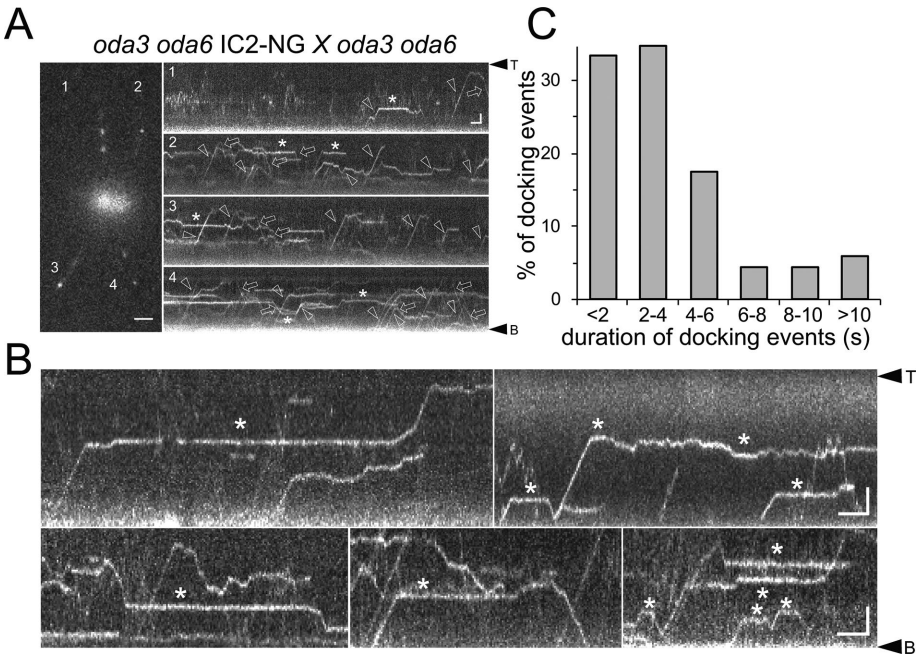

FIGURE 8: ODAs transiently dock in *oda3* flagella. (A) Still image and kymograms (1–4) of an *oda3 oda6* × *oda3 oda6* IC2-NG zygote. Arrows, retrograde transport; arrowheads, anterograde transports; asterisks, transiently stationary particles. Bars = 2 µm and 2 s. (B) Kymograms showing transient docking events of IC2-NG. Bars = 2 µm and 2 s. (C) Distribution of the duration of ODA transient docking events in *oda3* flagella (n = 69 docking events).

Takada *et al.*, 2002; Owa *et al.*, 2014). More recently, however, it was shown that in the absence of the DC ODAs still bind with a 24-nm repeat to microtubules, including microtubules assembled in vitro from brain tubulin (Oda *et al.*, 2016). In vivo imaging revealed that ODAs transiently bind to *oda3* flagella partially reconciling these apparently contradictory observations. After unloading from IFT, ODAs often dock instantaneously to *oda3* flagella just as observed during the rescue of *oda6* flagella. However, stable docking of ODAs in vivo requires the DC, supporting the notion that the DC stabilizes ODA–microtubule interaction (Oda *et al.*, 2016).

Low processivity of ODA transport could support ODA maintenance

In Figure 9, we compare the transport characteristics of IC2-NG/ODAs (O) to those of GFP-tagged versions of the dynein regulatory complex protein DRC4 (D), the radial spoke protein RSP4 (R), and the main structural axonemal protein tubulin (T). Tubulin interacts with the N-terminal domains of IFT protein IFT81 and IFT74 while ODA transport involves the head domain of IFT46. In extension, different axonemal proteins will bind to distinct sites of the IFT particle or train and each IFT–cargo complex will have its individual equilibrium and time constant. In comparison to the other axonemal cargoes, the transport of IC2-NG is of low processivity with less than one-third of the transports reaching the flagellar tip in one run from the base. However, IC2-NG released from IFT and diffusing inside the flagellum quickly reassociates to IFT trains. The formation of IFT–cargo complexes resembles a second-order reaction depending on the concentrations of the cargo and of binding sites on IFT, whereas complex fragmentation is a first-order reaction depending on the stability of the specific IFT–cargo complex. This concept explains the on-off behavior of cargoes along the flagellar shaft; it does not exclude that loading at the base and unloading at the tip are subjected to additional regulations. Unloading of axonemal proteins at the tip, for example, has been linked to the fragmentation of IFT trains during the transition from anterograde to retrograde traffic (Wren *et al.*, 2013; Chien *et al.*, 2017).

The transport of IC2-NG is of low processivity, bidirectional, and relatively frequent in full-length flagella. These features likely explain the pattern by which ODAs are added simultaneously along the length of flagella lacking them during zygotic rescue. However, zygotic repair of flagella is of little biological relevance and during flagellar growth all axonemal building blocks are needed at the flagellar tip. The distribution of unloading sites suggests that most ODAs will be transported directly to the tip while flagella are short but the chance of transport interruptions and retrograde transport of the unloaded ODAs will increase as flagella elongate. Thus, the transport characteristics of ODAs (and to a lesser extent those of RSPs and DRC4) could delay the addition of axonemal substructures to the tip of elongating cilia. Indeed, ultrastructural analysis revealed the absence of some ODAs and of other axonemal substructures in the subdistal region of growing flagella (Lechtreck *et al.*, 2013; Hoog *et al.*, 2014).

During flagellar maintenance, axonemal proteins will be exchanged with proteins newly imported into cilia (Stephens, 1994; Song and Dentler, 2001). The exchange of tubulin, which is almost exclusively transported to the tip, is essentially restricted to the flagellar tip (Marshall and Rosenbaum, 2001; Harris *et al.*, 2016). Incorporation of GFP-RSP4 and GFP-DRC4, which are both transported more processively and less retrogradely than IC2-NG, occurs preferably at the tip with little exchange along the length of flagella (Wren *et al.*, 2013; Lechtreck *et al.*, 2018). The incorporation of IC2-NG during maintenance of wild-type flagella, however, occurs with a higher frequency and along the length of the flagella, a pattern resembling that of ODA assembly onto ODA-deficient flagella. Premature unloading of cargoes from IFT could ensure rapid availability of proteins to replace lost ones. Thus, the transport characteristics of IC2-NG appear to match the pattern of ODA exchange in full-length cilia. The limited data available suggest a possible correlation between the processivity and retrograde frequency of transport and the rate of exchange of axonemal subunits in full-length cilia. We propose that the stability of the different IFT–cargo complexes has evolved to ensure optimal cargo delivery during cilia assembly and maintenance.

MATERIALS AND METHODS

Strains and culture conditions

C. reinhardtii was maintained in modified M medium at 24°C with a light/dark cycle of 14:10 h (www.chlamycollection.org/methods/media-recipes/minimal-or-m-medium-and-derivatives-sager-granick/). For flagella isolation, cultures were aerated with air supplemented with 0.5% CO_2. For gamete generation, cells were resuspended in M without nitrogen (M – N), and aerated for 15–18 h in constant light. Then, cells were incubated in 20% M – N with 10 mM HEPES, pH 7, for 3 h in constant light with agitation. After mixing of

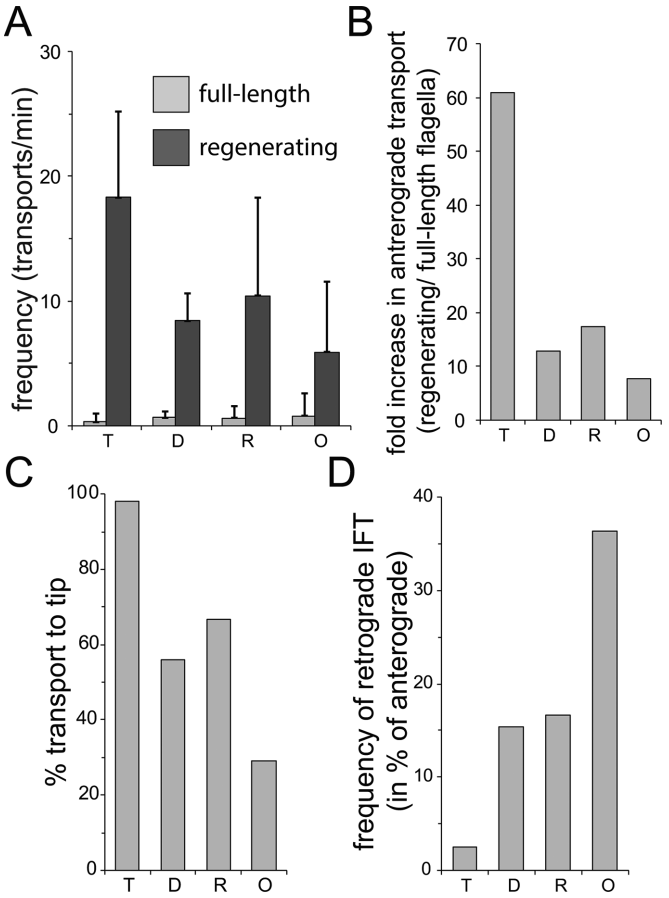

FIGURE 9: Axonemal proteins show distinct transport characteristics. Analysis of transport data for GFP-tagged tubulin (T), DRC4 (D), RSP4 (R), and IC2 (O). (A) Frequency of anterograde transport in full-length and regenerating flagella. (B) Ratio of the anterograde transport frequencies between regenerating and full-length flagella. (C) Share of transports that move processively from the flagellar base to the tip. The data for tubulin (T) are in parts based on regenerating flagella because its transport frequency is low in full-length flagella. (D) Frequency of retrograde transports expressed in % of the frequency of anterograde transports.

the gametes of opposite mating type, 15 mM dibutyryl-cAMP (Sigma-Aldrich) was added in some experiments to promote zygote formation (Pasquale and Goodenough, 1987). The following strains were used in this study: *ift20-1* IFT20-mCherry (Lechtreck *et al.*, 2009), *oda16-2* (Ahmed and Mitchell, 2005), and *ift46-1 IFT46ΔN* (Hou and Witman, 2017); CC-125 and CC-621 were used as wild-type strains. All other strains have been previously described and are available at the Chlamydomonas Resource Center (www.chlamycollection.org/).

Transgenic strain generation

A plasmid construct expressing NG fused to the C-terminus of IC2 (IC2-NG) was generated by Gibson overlap insertion of NG coding sequences (synthesized using the *Chlamydomonas* codon bias by IDT) into a *Bam*HI restriction site, as described previously for generation of Myc-tagged IC2 (Desai *et al.*, 2015). This plasmid was cotransformed along with ARG plasmid pJD67 into a slow-swimming *oda6 arg7* strain and initial transformants were selected for arginine autotrophy. Transformants with rescued motility were screened by whole cell protein blot with anti-IC2 for expression of IC2-NG. A single transformant with expression levels similar to the endogenous IC2 was used for all subsequent work, and the IC2-NG locus was then introduced through standard genetics into other mutant backgrounds. In all cases, those mutant backgrounds included *oda6*, such that all IC2-NG transgene expressing strains lack an endogenous source of IC2 expression. For each cross, 20–30 tetrads were dissected. Progeny with the expected motility phenotype were further verified for correct genotype through additional whole cell sample Western blots for IC2-NG expression, and through dikaryon rescue experiments to verify the presence of the expected *oda* mutant loci (*oda3*, *oda6*, *oda8*, *oda10*, *oda16*). Rescue in dikaryons was monitored through observation of changes in swimming velocity and through epifluorescent imaging of IC2-NG expression in flagella.

Flagellar isolation and Western blot

To isolate flagella for protein analysis, we followed a protocol described by Witman (1986). In brief, cells were concentrated and washed in 10 mM HEPES, pH 7.4, resuspended in HMS at 4°C (10 mM HEPES, 5 mM $MgSO_4$, and 4% sucrose) and deflagellated by adding dibucaine to a final concentration of 4.17 mM (Sigma-Aldrich) and repeated pipetting. Flagella were separated from cell bodies by centrifugation, collected from the supernatant by centrifugation, and resuspended in HMEK (30 mM HEPES, 5 mM $MgSO_4$, 25 mM KCl, and 0.5 mM ethylene glycol-bis(β-aminoethyl ether)-*N*,*N*,*N*′,*N*′-tetraacetic acid [EGTA]) with protease inhibitor cocktail (Sigma-Aldrich). For Western blotting, SDS–PAGE sample buffer was added to flagella samples and samples were incubated at 85°C for 10 min. The following primary antibodies were used: mouse anti-IC2 (1:1000; King and Witman, 1990), mouse anti-IFT81 (1:1000; Cole *et al.*, 1998), rabbit anti-ODA16 (1:200; Ahmed and Mitchell, 2005), and mouse anti-NG (1:1500; Chromotek). Western blots were developed using anti-mouse and anti-rabbit immunoglobulins G conjugated to horseradish peroxidase (Invitrogen) and chemiluminescence substrate (Michigan Diagnostics). Images were captured using a BioRad Gel Doc imaging system.

Flagellar regeneration

For flagella regeneration, cells in M medium were deflagellated by pH shock (~pH 4.3 for ~30 s), pelleted, and resuspended in fresh M medium. Flagella regrowth was allowed to proceed at room temperature under constant light and agitation. To delay flagella regrowth, cells were kept on ice until needed.

In vivo microscopy

For in vivo imaging, a Nikon Eclipse Ti-U inverted microscope equipped with a 60×/1.49 numerical aperture (NA) TIRF objective and a through-the-objective TIRF illumination system was used. Excitation light was provided by 75-mW, 561-nm and 40-mW, 488-nm diode lasers (Spectraphysics), and filtered by a Nikon GFP/mCherry TIRF filter cube (Lechtreck, 2013, 2016). The two-color emission was separated by using an image splitting device (Photometrics DualView2), and documented at 10 frames/s using an EMCCD camera (Andor iXon X3 DU897) and the Elements software package (Nikon). For photobleaching the entire flagellum, the laser intensity of the 488-nm laser was increased to 10% for 4–10 s. For photobleaching a specific area, a focused 488-nm laser beam was passed through the specimen in epifluorescence mode. To prepare the observation chamber, 10 µl of cells was placed on a 24 × 60 mm no. 1.5 coverslip previously applied with a ring of petroleum jelly. The cells were allowed to settle for ~1–10 min, mixed with an equal volume of 10 mM HEPES and 6.25 mM EGTA (pH 7.4) under a 22 × 22 mm no. 1.5 coverslip. The images were analyzed and kymograms and walking

averages were generated in FIJI (= ImageJ; National Institutes of Health). Merged images or kymograms were produced using Photoshop and figures were assembled in Illustrator (Adobe).

Immunofluorescence microscopy

For immunofluorescence microscopy, cells were fixed in 3% formaldehyde/0.1% Nonidet P-40 in HMEK and allowed to settle onto coated multiwall slides for 2 min followed by submersion in –20°C methanol for ~4 min. After air-drying, the slides were washed with phosphate-buffered saline (PBS), and blocked 2% bovine serum albumin (BSA) in PBS. The following primary antibodies and dilutions were used: mouse anti-IC2 (1:4) and rabbit anti-ODA16 (1:5). Specimens were incubated overnight at 4°C with primary antibodies in 2% BSA in PBS, and subsequently with secondary antibodies linked to Alexa Fluor 488 or 568 (1:1000; Invitrogen) for 90 min at room temperature. Specimens were mounted with ProlongGold (Invitrogen). Images were captured using a EMCCD camera (Andor iXon X3 DU897) and the Elements software package (Nikon) on a Nikon Eclipse Ti-U inverted microscope equipped with a 40×/0.75 NA objective (Nikon). Image brightness and contrast were adjusted using Photoshop (CC 2017; Adobe) and figures were assembled using Illustrator (CC 2017; Adobe).

ACKNOWLEDGMENTS

We thank Yuqing Hou and George Witman (University of Massachusetts Medical School) for kindly providing the *ift46 IFT46ΔN* strain. Judy Freshour provided technical assistance. This study was supported by the National Institutes of Health (R01GM110413 to K.L.). The content is solely the responsibility of the authors and does not necessarily represent the official views of the National Institutes of Health.

REFERENCES

Ahmed NT, Gao C, Lucker BF, Cole DG, Mitchell DR (2008). ODA16 aids axonemal outer row dynein assembly through an interaction with the intraflagellar transport machinery. J Cell Biol 183, 313–322.

Ahmed NT, Mitchell DR (2005). ODA16p, a *Chlamydomonas* flagellar protein needed for dynein assembly. Mol Biol Cell 16, 5004–5012.

Bhogaraju S, Cajanek L, Fort C, Blisnick T, Weber K, Taschner M, Mizuno N, Lamla S, Bastin P, Nigg EA, Lorentzen E (2013). Molecular basis of tubulin transport within the cilium by IFT74 and IFT81. Science 341, 1009–1012.

Bower R, Tritschler D, Vanderwaal K, Perrone CA, Mueller J, Fox L, Sale WS, Porter ME (2013). The N-DRC forms a conserved biochemical complex that maintains outer doublet alignment and limits microtubule sliding in motile axonemes. Mol Biol Cell 24, 1134–1152.

Brokaw CJ (1994). Control of flagellar bending: a new agenda based on dynein diversity. Cell Motil Cytoskeleton 28, 199–204.

Casey DM, Inaba K, Pazour GJ, Takada S, Wakabayashi K, Wilkerson CG, Kamiya R, Witman GB (2003). DC3, the 21-kDa subunit of the outer dynein arm-docking complex (ODA-DC), is a novel EF-hand protein important for assembly of both the outer arm and the ODA-DC. Mol Biol Cell 14, 3650–3663.

Chien A, Shih SM, Bower R, Tritschler D, Porter ME, Yildiz A (2017). Dynamics of the IFT machinery at the ciliary tip. Elife 6, e28606.

Cole DG, Diener DR, Himelblau AL, Beech PL, Fuster JC, Rosenbaum JL (1998). *Chlamydomonas* kinesin-II-dependent intraflagellar transport (IFT): IFT particles contain proteins required for ciliary assembly in *Caenorhabditis elegans* sensory neurons. J Cell Biol 141, 993–1008.

Craft JM, Harris JA, Hyman S, Kner P, Lechtreck KF (2015). Tubulin transport by IFT is upregulated during ciliary growth by a cilium-autonomous mechanism. J Cell Biol 208, 223–237.

Dean AB, Mitchell DR (2013). *Chlamydomonas* ODA10 is a conserved axonemal protein that plays a unique role in outer dynein arm assembly. Mol Biol Cell 24, 3689–3696.

Dean AB, Mitchell DR (2015). Late steps in cytoplasmic maturation of assembly-competent axonemal outer arm dynein in *Chlamydomonas* require interaction of ODA5 and ODA10 in a complex. Mol Biol Cell 26, 3596–3605.

Desai PB, Dean AB, Mitchell DR (2018). Cytoplasmic preassembly and trafficking of axonemal dyneins. In: Dyneins, Vol. 1, 2nd ed., ed. SM King, Cambridge, MA: Academic Press, 140–161.

Desai PB, Freshour JR, Mitchell DR (2015). *Chlamydomonas* axonemal dynein assembly locus ODA8 encodes a conserved flagellar protein needed for cytoplasmic maturation of outer dynein arm complexes. Cytoskeleton (Hoboken) 72, 16–28.

Dutcher SK (2014). The awesome power of dikaryons for studying flagella and basal bodies in *Chlamydomonas reinhardtii*. Cytoskeleton (Hoboken) 71, 79–94.

Fliegauf M, Benzing T, Omran H (2007). When cilia go bad: cilia defects and ciliopathies. Nat Rev Mol Cell Biol 8, 880–893.

Fowkes ME, Mitchell DR (1998). The role of preassembled cytoplasmic complexes in assembly of flagellar dynein subunits. Mol Biol Cell 9, 2337–2347.

Gao C, Wang G, Amack JD, Mitchell DR (2010). Oda16/Wdr69 is essential for axonemal dynein assembly and ciliary motility during zebrafish embryogenesis. Dev Dyn 239, 2190–2197.

Goodenough UW, Heuser JE (1982). Substructure of the outer dynein arm. J Cell Biol 95, 798–815.

Harris JA, Liu Y, Yang P, Kner P, Lechtreck KF (2016). Single particle imaging reveals IFT-independent transport and accumulation of EB1 in *Chlamydomonas* flagella. Mol Biol Cell 27, 295–307.

Hinrichs MH, Jalal A, Brenner B, Mandelkow E, Kumar S, Scholz T (2012). Tau protein diffuses along the microtubule lattice. J Biol Chem 287, 38559–38568.

Hoog JL, Lacomble S, O'Toole ET, Hoenger A, McIntosh JR, Gull K (2014). Modes of flagellar assembly in *Chlamydomonas reinhardtii* and *Trypanosoma brucei*. Elife 3, e01479.

Horani A, Ferkol TW, Dutcher SK, Brody SL (2016). Genetics and biology of primary ciliary dyskinesia. Paediatr Respir Rev 18, 18–24.

Horani A, Ustione A, Huang T, Firth AL, Pan J, Gunsten SP, Haspel JA, Piston DW, Brody SL (2018). Establishment of the early cilia preassembly protein complex during motile ciliogenesis. Proc Natl Acad Sci USA 115, E1221–E1228.

Hou Y, Qin H, Follit JA, Pazour GJ, Rosenbaum JL, Witman GB (2007). Functional analysis of an individual IFT protein: IFT46 is required for transport of outer dynein arms into flagella. J Cell Biol 176, 653–665.

Hou Y, Witman GB (2017). The N-terminus of IFT46 mediates intraflagellar transport of outer arm dynein and its cargo-adaptor ODA16. Mol Biol Cell 28, 2420–2433.

Hunter EL, Lechtreck K, Fu G, Hwang J, Lin H, Gokhale A, Alford LM, Lewis B, Yamamoto R, Kamiya R, *et al.* (2018). The IDA3 adapter, required for intraflagellar transport of I1 dynein, is regulated by ciliary length. Mol Biol Cell 29, 886–896.

Ibanez-Tallon I, Pagenstecher A, Fliegauf M, Olbrich H, Kispert A, Ketelsen UP, North A, Heintz N, Omran H (2004). Dysfunction of axonemal dynein heavy chain Mdnah5 inhibits ependymal flow and reveals a novel mechanism for hydrocephalus formation. Hum Mol Genet 13, 2133–2141.

Ide T, Owa M, King SM, Kamiya R, Wakabayashi K (2013). Protein-protein interactions between intermediate chains and the docking complex of *Chlamydomonas* flagellar outer arm dynein. FEBS Lett 587, 2143–2149.

Johnson KA, Rosenbaum JL (1992). Polarity of flagellar assembly in *Chlamydomonas*. J Cell Biol 119, 1605–1611.

Kamiya R (1988). Mutations at twelve independent loci result in absence of outer dynein arms in *Chylamydomonas reinhardtii*. J Cell Biol 107, 2253–2258.

Kee HL, Dishinger JF, Blasius TL, Liu CJ, Margolis B, Verhey KJ (2012). A size-exclusion permeability barrier and nucleoporins characterize a ciliary pore complex that regulates transport into cilia. Nat Cell Biol 14, 431–437.

King SM, Patel-King RS (2015). The oligomeric outer dynein arm assembly factor CCDC103 is tightly integrated within the ciliary axoneme and exhibits periodic binding to microtubules. J Biol Chem 290, 7388–7401.

King SM, Witman GB (1990). Localization of an intermediate chain of outer arm dynein by immunoelectron microscopy. J Biol Chem 265, 19807–19811.

Koutoulis A, Pazour GJ, Wilkerson CG, Inaba K, Sheng H, Takada S, Witman GB (1997). The *Chlamydomonas reinhardtii* ODA3 gene encodes a protein of the outer dynein arm docking complex. J Cell Biol 137, 1069–1080.

Kozminski KG, Johnson KA, Forscher P, Rosenbaum JL (1993). A motility in the eukaryotic flagellum unrelated to flagellar beating. Proc Natl Acad Sci USA 90, 5519–5523.

Lechtreck K, Mengoni I, Okivie B, Hilderhoff KB (2018). *In vivo* analyses of radial spoke transport, assembly, repair and maintenance. Cytoskeleton, doi: 10.1002/cm.21457.

Lechtreck KF (2013). In vivo imaging of IFT in *Chlamydomonas* flagella. Methods Enzymol 524, 265–284.
Lechtreck KF (2015). IFT-cargo interactions and protein transport in cilia. Trends Biochem Sci 40, 765–778.
Lechtreck KF (2016). Methods for studying movement of molecules within cilia. Methods Mol Biol 1454, 83–96.
Lechtreck KF, Gould TJ, Witman GB (2013). Flagellar central pair assembly in *Chlamydomonas reinhardtii*. Cilia 2, 15.
Lechtreck KF, Johnson EC, Sakai T, Cochran D, Ballif BA, Rush J, Pazour GJ, Ikebe M, Witman GB (2009). The *Chlamydomonas reinhardtii* BBSome is an IFT cargo required for export of specific signaling proteins from flagella. J Cell Biol 187, 1117–1132.
Lin YC, Niewiadomski P, Lin B, Nakamura H, Phua SC, Jiao J, Levchenko A, Inoue T, Rohatgi R (2013). Chemically inducible diffusion trap at cilia reveals molecular sieve-like barrier. Nat Chem Biol 9, 437–443.
Lin J, Okada K, Raytchev M, Smith MC, Nicastro D (2014). Structural mechanism of the dynein power stroke. Nat Cell Biol 16, 479–485.
Liu P, Lechtreck KF (2018). The Bardet-Biedl syndrome protein complex is an adapter expanding the cargo range of intraflagellar transport trains for ciliary export. Proc Natl Acad Sci USA 115, E934–E943.
Marshall WF, Rosenbaum JL (2001). Intraflagellar transport balances continuous turnover of outer doublet microtubules: implications for flagellar length control. J Cell Biol 155, 405–414.
Mirra V, Werner C, Santamaria F (2017). Primary ciliary dyskinesia: an update on clinical aspects, genetics, diagnosis, and future treatment strategies. Front Pediatr 5, 135.
Nonaka S, Tanaka Y, Okada Y, Takeda S, Harada A, Kanai Y, Kido M, Hirokawa N (1998). Randomization of left-right asymmetry due to loss of nodal cilia generating leftward flow of extraembryonic fluid in mice lacking KIF3B motor protein. Cell 95, 829–837.
Oda T, Abe T, Yanagisawa H, Kikkawa M (2016). Docking-complex-independent alignment of *Chlamydomonas* outer dynein arms with 24-nm periodicity in vitro. J Cell Sci 129, 1547–1551.
Omran H, Kobayashi D, Olbrich H, Tsukahara T, Loges NT, Hagiwara H, Zhang Q, Leblond G, O'Toole E, Hara C, *et al*. (2008). Ktu/PF13 is required for cytoplasmic pre-assembly of axonemal dyneins. Nature 456, 611–616.
Owa M, Furuta A, Usukura J, Arisaka F, King SM, Witman GB, Kamiya R, Wakabayashi K (2014). Cooperative binding of the outer arm-docking complex underlies the regular arrangement of outer arm dynein in the axoneme. Proc Natl Acad Sci USA 111, 9461–9466.
Pasquale SM, Goodenough UW (1987). Cyclic AMP functions as a primary sexual signal in gametes of *Chlamydomonas reinhardtii*. J Cell Biol 105, 2279–2292.
Piperno G, Mead K, Henderson S (1996). Inner dynein arms but not outer dynein arms require the activity of kinesin homologue protein KHP1(FLA10) to reach the distal part of flagella in *Chlamydomonas*. J Cell Biol 133, 371–379.
Qin H, Diener DR, Geimer S, Cole DG, Rosenbaum JL (2004). Intraflagellar transport (IFT) cargo: IFT transports flagellar precursors to the tip and turnover products to the cell body. J Cell Biol 164, 255–266.
Ringo DL (1967). Flagellar motion and fine structure of the flagellar apparatus in *Chlamydomonas*. J Cell Biol 33, 543–571.
Rosenbaum JL, Moulder JE, Ringo DL (1969). Flagellar elongation and shortening in *Chlamydomonas*. The use of cycloheximide and colchicine to study the synthesis and assembly of flagellar proteins. J Cell Biol 41, 600–619.
Rosenbaum JL, Witman GB (2002). Intraflagellar transport. Nat Rev Mol Cell Biol 3, 813–825.
Satir P (1968). Studies on cilia. 3. Further studies on the cilium tip and a "sliding filament" model of ciliary motility. J Cell Biol 39, 77–94.
Song L, Dentler WL (2001). Flagellar protein dynamics in *Chlamydomonas*. J Biol Chem 276, 29754–29763.
Stepanek L, Pigino G (2016). Microtubule doublets are double-track railways for intraflagellar transport trains. Science 352, 721–724.
Stephan A, Vaughan S, Shaw MK, Gull K, McKean PG (2007). An essential quality control mechanism at the eukaryotic basal body prior to intraflagellar transport. Traffic 8, 1323–1330.
Stephens RE (1994). Tubulin and tektin in sea urchin embryonic cilia: pathways of protein incorporation during turnover and regeneration. J Cell Sci 107 (Pt 2), 683–692.
Takada S, Sakakibara H, Kamiya R (1992). Three-headed outer arm dynein from *Chlamydomonas* that can functionally combine with outer-arm-missing axonemes. J Biochem 111, 758–762.
Takada S, Wilkerson CG, Wakabayashi K, Kamiya R, Witman GB (2002). The outer dynein arm-docking complex: composition and characterization of a subunit (oda1) necessary for outer arm assembly. Mol Biol Cell 13, 1015–1029.
Taschner M, Mourao A, Awasthi M, Basquin J, Lorentzen E (2017). Structural basis of outer dynein arm intraflagellar transport by the transport adaptor protein ODA16 and the intraflagellar transport protein IFT46. J Biol Chem 292, 7462–7473.
Viswanadha R, Hunter EL, Yamamoto R, Wirschell M, Alford LM, Dutcher SK, Sale WS (2014). The ciliary inner dynein arm, I1 dynein, is assembled in the cytoplasm and transported by IFT before axonemal docking. Cytoskeleton (Hoboken) 71, 573–586.
Wakabayashi K, Takada S, Witman GB, Kamiya R (2001). Transport and arrangement of the outer-dynein-arm docking complex in the flagella of *Chlamydomonas* mutants that lack outer dynein arms. Cell Motil Cytoskeleton 48, 277–286.
Wingfield JL, Mengoni I, Bomberger H, Jiang YY, Walsh JD, Brown JM, Picariello T, Cochran DA, Zhu B, Pan J, *et al*. (2017). IFT trains in different stages of assembly queue at the ciliary base for consecutive release into the cilium. Elife 6, e26609.
Witman, G.B. (1986). Isolation of *Chlamydomonas* flagella and flagellar axonemes. Methods Enzymol 134, 280–290.
Wren KN, Craft JM, Tritschler D, Schauer A, Patel DK, Smith EF, Porter ME, Kner P, Lechtreck KF (2013). A differential cargo-loading model of ciliary length regulation by IFT. Curr Biol 23, 2463–2471.
Zimmermann D, Abdel Motaal B, Voith von Voithenberg L, Schliwa M, Okten Z (2011). Diffusion of myosin V on microtubules: a fine-tuned interaction for which E-hooks are dispensable. PLoS One 6, e25473.